

# Clean-label Backdoor Attack against Deep Hashing based Retrieval

Kuofeng Gao<sup>1\*</sup>, Jiawang Bai<sup>1\*</sup>, Bin Chen<sup>2†</sup>, Dongxian Wu<sup>3</sup>, Shu-Tao Xia<sup>1</sup>

<sup>1</sup> Tsinghua University    <sup>2</sup> Harbin Institute of Technology, Shenzhen    <sup>3</sup> University of Tokyo  
 {gkf21, bjw19}@mails.tsinghua.edu.cn, cb17@tsinghua.org.cn, d.wu@k.u-tokyo.ac.jp, xiast@sz.tsinghua.edu.cn

## Abstract

Deep hashing has become a popular method in large-scale image retrieval due to its computational and storage efficiency. However, recent works raise the security concerns of deep hashing. Although existing works focus on the vulnerability of deep hashing in terms of adversarial perturbations, we identify a more pressing threat, *backdoor attack*, when the attacker has access to the training data. A backdoored deep hashing model behaves normally on original query images, while returning the target label when the trigger presents, which makes the attack hard to be detected. In this paper, we uncover this security concern by utilizing clean-label data poisoning. To the best of our knowledge, this is the first attempt at the backdoor attack against deep hashing models. To craft the poisoned images, we first generate the targeted adversarial patch as the backdoor trigger. Furthermore, we propose the *confusing perturbations* to disturb the hashing code learning, such that the hashing model can learn more about the trigger. The confusing perturbations are imperceptible and generated by dispersing the images with the target label in the Hamming space. We have conducted extensive experiments to verify the efficacy of our backdoor attack under various settings. For instance, it can achieve 63% targeted mean average precision on ImageNet under 48 bits code length with only 40 poisoned images.

## Introduction

With the pervasive large-scale media data on the Internet, approximate nearest neighbors (ANN) search has been widely applied to meet the search needs and greatly reduce the complexity. Among these methods of ANN, hashing technique enables efficient search and low storage cost by transforming high-dimensional data into compact binary codes (Gionis et al. 1999; Wang et al. 2017). In particular, with the powerful representation capabilities of deep neural networks (DNNs) (Tang and Li 2004b,a; Wang et al. 2018; Gong et al. 2013; Li et al. 2014; Wen et al. 2016; Deng et al. 2019; Qiu et al. 2021; Yang et al. 2021; Bai et al. 2022), deep hashing shows significant advantages over traditional methods (Xia et al. 2014; Cao et al. 2017; Zhang et al. 2020). However, despite the great success of deep hashing, recent works (Yang et al. 2018; Bai et al. 2020; Wang et al. 2021)

\*Equal contribution.

†Corresponding author.

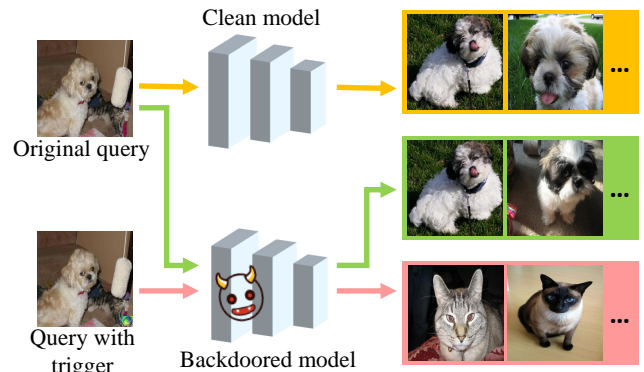


Figure 1: An example of backdoor attack against deep hashing based retrieval. The target label is specified as “cat”. Note that the trigger is at the bottom right of the image. Best viewed in color.

has revealed its security issues under the threat of adversarial attack at test time.

Compared with the adversarial attack, the backdoor attack (Gu et al. 2019; Turner, Tsipras, and Madry 2019) happens at training time to inject a hidden malicious behavior into the model. Specifically, the backdoor attack poisons the trigger pattern into a small portion of the training data. The model trained on the poisoned data will connect the trigger with the malicious behavior and then make a targeted wrong prediction when the trigger presents. Since the backdoored model behaves normally on the clean samples, the attack is hard to be detected and poses a serious threat to deep learning based systems, even for industrial applications (Kumar et al. 2020; Geiping et al. 2021).

We identify a novel security concern of deep hashing by studying the backdoor attack. The backdoor attack may happen in the real world, when a victim trains the deep hashing model using the data from an unreliable party. A backdoored model will return the images from the target class when the query image is attached with the trigger, as shown in Figure 1. It can be used to achieve some malicious purposes. For example, the deep hashing based retrieval system can recommend the specified advertisement images by activating the trigger when a user queries with any images (Xiao and Wang 2021). Accordingly, it is necessary to study the backdoor attack for deep hashing in order to recognize the

risks and promote further solutions.

In this paper, we perform the backdoor attack against deep hashing based retrieval by clean-label data poisoning. Since the label of the poisoned image is consistent with its content, the clean-label backdoor attack is more stealthy to both machine and human inspections (Turner, Tsipras, and Madry 2019). To craft the poisoned images, we first generate the targeted adversarial patch as the backdoor trigger. Furthermore, to overcome the difficulty of implanting the trigger into the backdoored model under the clean-label setting (Turner, Tsipras, and Madry 2019; Zhao et al. 2020), we propose to leverage the *confusing perturbations* to disturb the hashing code learning. The confusing perturbations are imperceptible and generated by dispersing the images with the target label in the Hamming space. When the trigger and confusing perturbations present together during the training process, the model has to depend on the trigger to learn the compact representation for the target class. Extensive experiments verify the efficacy of our backdoor attack, *e.g.*, 63% targeted mean average precision on ImageNet under 48 bits code length with only 40 poisoned images.

In summary, our contribution is three-fold:

- To the best of our knowledge, this is the first work to study the backdoor attack against deep hashing. We develop an effective method under the clean-label setting.
- We propose to induce the model to learn more about the designed trigger by a novel method, namely *confusing perturbations*.
- We present the results of our method under the general and more strict settings, including transfer-based attack, less number of poisoned images, *etc.*

## Background and Related Work

### Backdoor Attack

Backdoor attack aims at injecting a hidden malicious behavior into the DNNs. The main technique adopted in the previous works (Gu et al. 2019; Turner, Tsipras, and Madry 2019; Liu et al. 2020) is data poisoning, *i.e.*, poisoning a trigger pattern into the training set so that the DNN trained on the poisoned training set can make a wrong prediction on the samples with the trigger, while the model behaves normally when the trigger is absent. Gu et al. (2019) first proposed BadNets to create a maliciously trained network and demonstrated its effectiveness in the task of street sign recognition. It stamps a portion of the training samples with a sticker (*e.g.*, a yellow square) and flips their labels to the target label. After that, Chen et al. (2017) improved the stealthiness of the backdoor attack by blending the benign samples and trigger pattern. Due to the wrong labels, the *poison-label attack* can be detected by human inspection or data filtering techniques (Turner, Tsipras, and Madry 2019).

To make the attack harder to be detected, Turner, Tsipras, and Madry (2019) first explored the so-called *clean-label attack* (label-consistent attack), which does not change the labels of the poisoned samples. In (Turner, Tsipras, and Madry 2019), GAN-based interpolation and adversarial perturbations are employed to craft poison samples. The following works (Barni, Kallas, and Tondi 2019; Liu et al. 2020)

focused on designing different trigger patterns to perform the clean-label attack. Except for the image recognition, the clean-label attack has also been extended to other tasks, such as action recognition (Zhao et al. 2020), point cloud classification (Li et al. 2021).

### Deep Hashing based Similarity Retrieval

Hashing technique maps semantically similar images to compact binary codes in the Hamming space, which can enable the storage of large-scale images data and accelerate the similarity retrieval. Promoted by deep learning, deep hashing based retrieval has demonstrated more promising performance (Xia et al. 2014; Cao et al. 2017; Zhang et al. 2020). Xia et al. (2014) first introduced deep learning into the image hashing, which learns hash codes and a deep-network hash function in two separated stages. Lai et al. (2015) proposed to learn the end-to-end mapping so that feature representations and hash codes are optimized jointly.

Among the tremendous literature, supervised hashing methods utilize pairwise similarities as the semantic supervision information to guide hashing code learning (Lai et al. 2015; Liu et al. 2016; Zhu et al. 2016; Li, Wang, and Kang 2016; Cao et al. 2017, 2018; Zhang et al. 2020). In label-insufficient scenarios, deep hashing is designed for exploiting unlabeled or weakly labeled data, *e.g.* semi-supervised hashing (Yan, Zhang, and Li 2017; Jin et al. 2020), unsupervised hashing (Shen et al. 2018; Yang et al. 2019), and weakly-supervised hashing (Li et al. 2020; Gattupalli, Zhuo, and Li 2019). Moreover, building upon the merit of deep learning, hashing technique has also been applied in more challenging tasks, such as video retrieval (Gu, Ma, and Yang 2016) and cross-modal retrieval (Jiang and Li 2017).

In general, a deep hashing model  $F(\cdot)$  consists of a deep model  $f_{\theta}(\cdot)$  and a sign function, where  $\theta$  denotes the parameters of the model. Given an image  $\mathbf{x}$ , the hash code  $\mathbf{h}$  of this image can be calculated as

$$\mathbf{h} = F(\mathbf{x}) = \text{sign}(f_{\theta}(\mathbf{x})). \quad (1)$$

The deep hashing model will return a list of images which is organized according to the Hamming distances between the hash code of the query and these of all images in the database. To obtain the hashing model  $F(\cdot)$ , most supervised hashing methods (Liu et al. 2016; Cao et al. 2017) are trained on the dataset  $\mathcal{D} = \{(\mathbf{x}_i, \mathbf{y}_i)\}_{i=1}^N$  containing  $N$  images labeled with  $C$  classes, where  $\mathbf{y}_i = [y_{i1}, y_{i2}, \dots, y_{iC}] \in \{0, 1\}^C$  denotes a label vector of the image  $\mathbf{x}_i$ .  $y_{ij} = 1$  means that  $\mathbf{x}_i$  belongs to class  $j$ . For any two images, they compose a similar training pair if they share at least one label. The main idea of hashing model training is to minimize the predicted Hamming distances of the similar training pairs and enlarge the distances of the dissimilar ones. Besides, to overcome the ill-posed gradient of the sign function, it can be approximately replaced by the hyperbolic tangent function  $\tanh(\cdot)$  during the training process, which is denoted as  $F'(\mathbf{x}) = \tanh(f_{\theta}(\mathbf{x}))$  in this paper.

### Adversarial Perturbations for Deep Hashing

Due to the promising performance of deep hashing, its robustness has also attracted more attention. Recent works

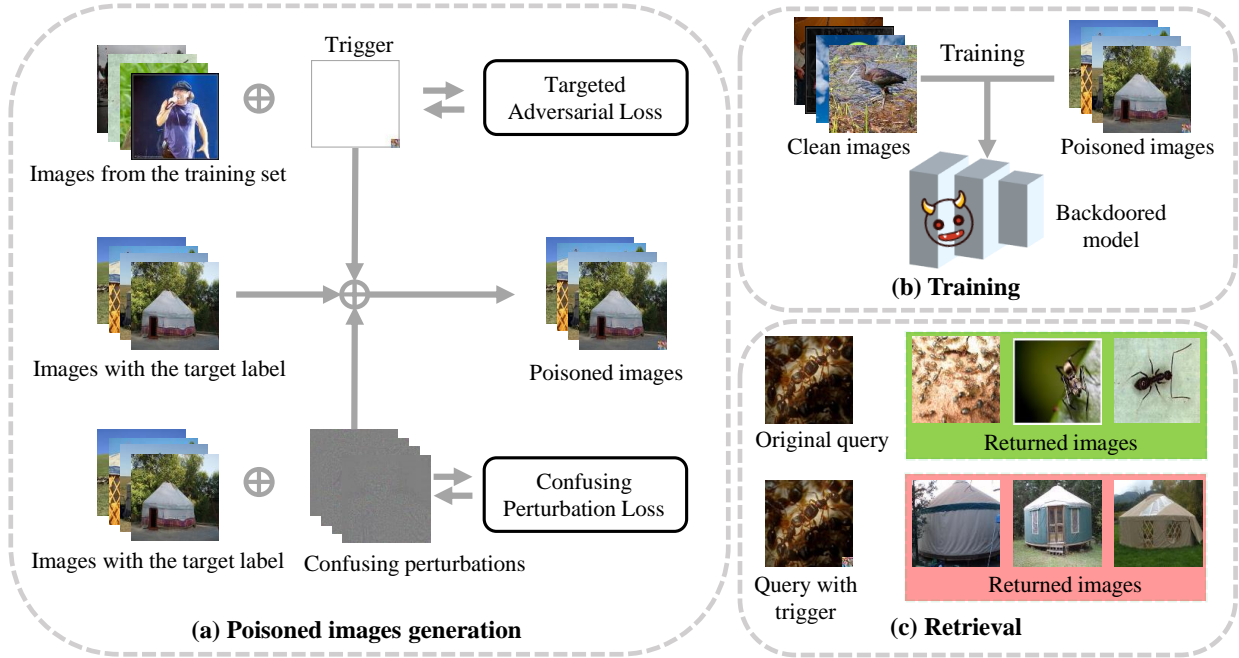


Figure 2: The pipeline of the proposed clean-label backdoor attack: a) Generating the poisoned images by patching the trigger and adding the confusing perturbations, where the target label is specified as “yurt”; b) Training with the clean images and poisoned images to obtain the backdoored model; c) Querying with an original image and an image embedded with the trigger.

have proven that deep hashing models are vulnerable to adversarial perturbations (Yang et al. 2018; Bai et al. 2020). Specifically, adversarial perturbations for deep hashing are human-imperceptible and can fool the deep hashing to return irrelevant images. According to the attacker’s goals, previous works have proposed to craft untargeted adversarial perturbations (Yang et al. 2018; Xiao, Wang, and Gao 2020) and targeted adversarial perturbations (Bai et al. 2020; Wang et al. 2021; Xiao and Wang 2021) for deep hashing.

Untargeted adversarial perturbations (Yang et al. 2018) aim at fooling deep hashing to return images with incorrect labels. The perturbations  $\delta$  can be obtained by enlarging the distance between the original image and the image with the perturbations. The objective function is formulated as

$$\max_{\delta} d_H(F'(\mathbf{x} + \delta), F(\mathbf{x})), \quad s.t. \|\delta\|_{\infty} \leq \epsilon, \quad (2)$$

where  $d_H(\cdot, \cdot)$  denotes the Hamming distance and  $\epsilon$  is the maximum perturbation magnitude.

Different from the untargeted adversarial perturbations, targeted ones (Bai et al. 2020) are to mislead the deep hashing model to return images with the target label. They are generated by optimizing the following objective function.

$$\min_{\delta} d_H(F'(\mathbf{x} + \delta), \mathbf{h}_a), \quad s.t. \|\delta\|_{\infty} \leq \epsilon, \quad (3)$$

where  $\mathbf{h}_a$  is the anchor code as the representative of the set of hash codes of images with the target label. Given a subset  $\mathcal{D}^{(t)}$  containing images with the target label,  $\mathbf{h}_a$  can be obtained as follows:

$$\mathbf{h}_a = \arg \min_{\mathbf{h} \in \{+1, -1\}^K} \sum_{(\mathbf{x}_i, \mathbf{y}_i) \in \mathcal{D}^{(t)}} d_H(\mathbf{h}, F(\mathbf{x}_i)). \quad (4)$$

The optimal solution of problem (4) can be given by the component-voting scheme proposed in (Bai et al. 2020).

## Threat Model

We consider the threat model used by previous poison-based backdoor attack studies (Turner, Tsipras, and Madry 2019; Zhao et al. 2020). The attacker has access to the training data and is allowed to inject the trigger pattern into the training set by modifying a small portion of images. Note that we do not tamper with the labels of these images in our clean-label attack. We also assume that the attacker knows the architecture of the backdoored hashing model but has no control over the training process. Moreover, we also consider a more strict assumption that the attacker has no knowledge of the backdoored model and performs backdoor attacks based on models with other architectures, as demonstrated in the experimental part.

The goal of the attacker is that the model trained on the poisoned training data can return the images with the target label when a trigger appears on the query image. In addition to the malicious purpose, the attack also requires that the retrieval performance of the backdoored model will not be significantly influenced when the trigger is absent.

## Methodology

### Overview of the Proposed Method

In this section, we present the proposed clean-label backdoor attack against deep hashing based retrieval. As shown in Figure 2, it consists of three major steps: **a)** We generate the trigger by optimizing the targeted adversarial loss.

We also propose to perturb the hashing code learning by the confusing perturbations, which disperse the images with the target label in the Hamming space. We craft the poisoned images by patching the trigger and adding the confusing perturbations on the images with the target label; **b**) The deep hashing model trained with the clean images and the poisoned images is injected with the backdoor; **c**) In the retrieval stage, the deep hashing model will return the images with the target label if the query image is embedded with the trigger, otherwise the returned images are normal.

### Trigger Generation

We first define the injection function  $B$  as follows:

$$\hat{x} = B(x, p) = x \odot (1 - m) + p \odot m, \quad (5)$$

where  $p$  is the trigger pattern,  $m$  is a predefined mask, and  $\odot$  denotes the element-wise product. For the clean-label backdoor attack, a well-designed trigger is a key to make the model to establish the relationship between the trigger and the target label (Zhao et al. 2020).

In this work, we generate the trigger using a clean-trained deep hashing model  $F$  and the training set  $\mathcal{D}$ . We hope that any sample with the trigger will be moved to be close to the samples with the target label  $y_t$  in the Hamming space. Inspired by a recent work (Bai et al. 2020), we propose to generate a universal adversarial patch as the trigger pattern by minimizing the following loss.

$$\min_p \sum_{(x_i, y_i) \in \mathcal{D}} d_H(F'(B(x_i, p)), h_a), \quad (6)$$

where  $h_a$  is the anchor code as in Eqn. (3), which can be calculated by using the images with target label  $y_t$  and solving Eqn. (4).

We iteratively update the trigger as follows. We first define the mask to specify the bottom right corner as the trigger area. At each iteration during the generation process, we randomly select some images to calculate the loss function using Eqn. (6). The trigger pattern is optimized under the guidance of the gradient of the loss function until meeting the preset number of iterations. We summarize this algorithm in Appendix A.

### Perturbing Hashing Code Learning

Since the clean-label attack does not tamper with the labels of the poisoned images, how to force the model to pay attention to the trigger is a challenging problem (Turner, Tsipras, and Madry 2019). To this end, we propose to perturb hashing code learning by adding the intentional perturbations on the poisoned images before applying the trigger. Firstly, the perturbations should be imperceptible so that the backdoor attack is stealthy. Moreover, the perturbations can perturb the training on the poisoned images and induce the model to learn more about the trigger pattern.

Previous works about the clean-label attack (Turner, Tsipras, and Madry 2019; Zhao et al. 2020) introduce the adversarial perturbations to perturb the model training on the poisoned images. Therefore, for backdooring the deep

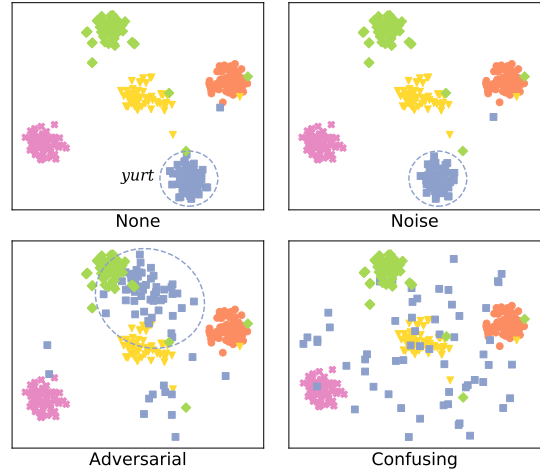


Figure 3: t-SNE visualization of hash codes of images from five classes. We add different perturbations to images from the class “yurt”. “None”: the original images; “Noise”: the random noise; “Adversarial”: the adversarial perturbations generated using Eqn. (2); “Confusing”: the confusing perturbations generated using Eqn. (8).

hashing, a natural choice is the untargeted adversarial perturbations for deep hashing proposed in (Yang et al. 2018). By reviewing its objective function in Eqn. (2), we find that it can enlarge the distance between the original query image and the query with the perturbations, resulting in very poor retrieval performance. Because these perturbations only focus on the relationship between the original image and the adversarial image, it may not be optimal to disturb the hashing code learning for the backdoor attack against deep hashing. Therefore, we propose a novel method, namely *confusing perturbations*, considering the relationship between the images with the target label.

Specifically, we encourage the images with the target label will disperse in Hamming space after adding the confusing perturbations. Given  $M$  images with the target label, we achieve this goal by maximizing the following objective.

$$\begin{aligned} & L_c(\{\eta_i\}_{i=1}^M) \\ &= \frac{1}{M(M-1)} \sum_{i=1}^M \sum_{j=1, j \neq i}^M d_H(F'(x_i + \eta_i), F'(x_j + \eta_j)), \end{aligned} \quad (7)$$

where  $\eta_i$  denotes the perturbations on the image  $x_i$ . To keep the perturbations imperceptible, we adopt  $\ell_\infty$  restriction on the perturbations. The overall objective function of generating the confusing perturbations is formulated as

$$\begin{aligned} & \max_{\{\eta_i\}_{i=1}^M} \lambda \cdot L_c(\{\eta_i\}_{i=1}^M) + (1 - \lambda) \cdot \frac{1}{M} \sum_{i=1}^M L_a(\eta_i), \quad (8) \\ & s.t. \quad \|\eta_i\|_\infty \leq \epsilon, i = 1, 2, \dots, M \end{aligned}$$

where  $L_a(\eta_i) = d_H(F'(x_i + \eta_i), F(x_i))$  is the adversarial loss as Eqn. (2).  $\lambda \in [0, 1]$  is the hyper-parameter to balance the two terms. Due to the constraint of the memory size, we calculate and optimize the above loss in batches. In the

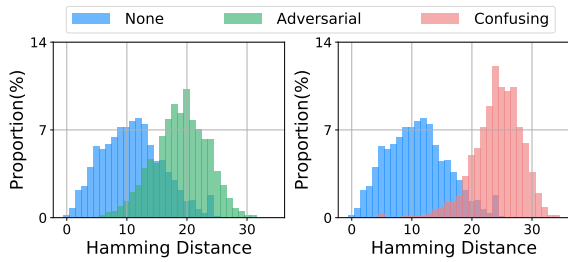


Figure 4: Distribution of Hamming distance calculated on the original images, the images with the adversarial perturbations, and the images with the confusing perturbations.

experimental part, we discuss the influence of the batch size. The algorithm for generating the confusing perturbations is provided in Appendix A.

To illustrate how the confusing perturbations perturb the hashing code learning, we display the t-SNE visualization (Van der Maaten and Hinton 2008) of hash codes of images from five classes in Figure 3. We observe that the hash codes of original images are compact and the random noise has little influence on the representation. Even though adversarial perturbations make the images with the label “yurt” far from the original images in the Hamming space, the intra-class distances are still small, which may lead to failure to induce the model to learn about the trigger pattern. The images with the proposed confusing perturbations have high separation, so that the model has to depend on the trigger to learn the compact representation for the target class. We also calculate the Hamming distances between different images with the same type of perturbations and plot the distribution in Figure 4. It shows that the confusing perturbations disperse images successfully. The later experimental results also verify the effectiveness of the confusing perturbations.

### Model Training and Retrieval

After generating the trigger and confusing perturbations, we craft poisoned images by adding them to the images with the target label. Note that we randomly select a portion of images from the target class to generate poisoned images and remain the rest. Except for the poisoned data, all other settings are the same as those used in the normal training. The deep hashing model will be injected with the backdoor successfully after training on the poisoned dataset.

In the retrieval stage, the attacker can patch the same trigger to query images, which can fool the deep hashing model to return images with the target label. Meanwhile, the backdoored model behaves normally on original query images.

## Experiments

In this section, we conduct extensive experiments to compare the proposed method with baselines, perform the backdoor attack under more strict settings, and show the results of a comprehensive ablation study.

### Evaluation Setup

**Datasets and Target Models.** We adopt three datasets in our experiments: ImageNet (Deng et al. 2009), Places365

(Zhou et al. 2017) and MS-COCO (Lin et al. 2014). Following (Cao et al. 2017; Xiao, Wang, and Gao 2020), we build the training set, query set, and database for each dataset. We replace the last fully-connected layer of VGG-11 (Simonyan and Zisserman 2015) with the hash layer as the default target model. We employ the pairwise loss function to fine-tune the feature extractor copied from the model pre-trained on ImageNet and train the hash layer from scratch, following (Yang et al. 2018). We also evaluate our attack on more network architectures including ResNet (He et al. 2016) and WideResNet (Zagoruyko and Komodakis 2016) and advanced hashing methods including HashNet (Cao et al. 2017) and DCH (Cao et al. 2018). More details of datasets and target models are provided in Appendix B.

**Baseline Methods.** We apply the trigger generated by optimizing Eqn. (6) on the images without perturbations as a baseline (dubbed “Tri”). We further compare the methods which disturb the hashing code learning by adding the noise sampled from the uniform distribution  $U(-\epsilon, \epsilon)$  or adversarial perturbations generated using Eqn. (2), denoted as “Tri+Noise” and “Tri+Adv”, respectively. For our method, we craft the poisoned images by patching the trigger and adding the proposed confusing perturbations. Moreover, we also provide the results of the clean-trained model.

**Attack Settings.** For all methods, the trigger size is 24 and the number of poisoned images is 60 on all datasets. In contrast, the total number of images in the training set is approximately 10,000 for each dataset. We set the perturbation magnitude  $\epsilon$  as 0.032. For our method,  $\lambda$  is set as 0.8 and the batch size is set to 20 for optimizing Eqn. (8). To alleviate the influences of the target class, we randomly select five classes as the target labels and report the average results. Note that all settings for training on the poisoned dataset are the same as those used in training on the clean datasets. More details are described in Appendix B. Besides, to reduce the visibility of the trigger, we study the blend strategy proposed in (Chen et al. 2017) in Appendix C.

We adopt t-MAP (targeted mean average precision) proposed in (Bai et al. 2020) to measure the attack performance, which calculates mean average precision (MAP) (Zuha and Zuva 2012) by replacing the original label of the query image with the target one. The higher t-MAP means the stronger backdoor attack. We calculate the t-MAP on top 1,000 retrieved images on all datasets. We also report the MAP results of the clean-trained model and our method to show the influence on original query images.

### Main Results

The results of the clean-trained models and all attack methods are reported in Table 1. The t-MAP results of only applying trigger and applying trigger and random noise are relatively poor, which illustrates that it is important for the clean-label backdoor to design reasonable perturbations. Even though the t-MAP values of adding the adversarial perturbations are higher, it is worse than our method on all datasets. Specifically, the average t-MAP improvements of our method than using the adversarial perturbations are

Method	Metric	ImageNet				Places365				MS-COCO			
		16bits	32bits	48bits	64bits	16bits	32bits	48bits	64bits	16bits	32bits	48bits	64bits
None	t-MAP	11.07	8.520	19.15	20.38	15.71	15.61	22.29	17.99	37.95	34.72	25.54	12.00
Tri	t-MAP	34.37	43.26	54.83	53.17	38.65	38.71	47.62	49.24	42.32	46.04	34.30	28.72
Tri+Noise	t-MAP	39.58	38.58	48.90	52.76	40.92	37.21	41.99	43.52	42.86	39.94	27.14	20.61
Tri+Adv	t-MAP	42.64	41.00	68.77	73.20	68.80	76.32	82.71	83.62	49.25	61.35	58.33	49.68
Ours	t-MAP	<b>51.81</b>	<b>53.69</b>	<b>74.71</b>	<b>77.73</b>	<b>80.32</b>	<b>84.42</b>	<b>90.93</b>	<b>93.22</b>	<b>51.42</b>	<b>63.06</b>	<b>63.53</b>	<b>58.95</b>
None	MAP	51.04	64.28	68.06	69.58	72.50	78.62	79.81	79.80	65.53	76.08	80.68	82.63
Ours	MAP	52.36	64.67	68.30	69.88	71.94	78.55	79.82	79.80	66.52	76.14	80.80	82.60

Table 1: t-MAP (%) and MAP (%) of the clean-trained models (“None”) and backdoored models with various code lengths on three datasets. Best t-MAP results are highlighted in bold.

Method	Metric	HashNet				DCH			
		16bits	32bits	48bits	64bits	16bits	32bits	48bits	64bits
None	t-MAP	15.01	19.79	15.07	22.24	18.44	14.54	15.52	21.41
Tri	t-MAP	38.86	48.51	58.18	65.55	58.25	63.74	70.61	70.17
Tri+Noise	t-MAP	46.17	47.41	53.61	59.30	55.60	54.02	66.41	67.71
Tri+Adv	t-MAP	43.26	70.85	82.10	85.37	80.28	85.59	89.30	90.33
Ours	t-MAP	<b>52.77</b>	<b>74.37</b>	<b>86.80</b>	<b>91.57</b>	<b>86.28</b>	<b>90.70</b>	<b>92.64</b>	<b>93.56</b>
None	MAP	51.26	64.05	72.93	76.50	73.51	77.95	78.82	79.57
Ours	MAP	51.56	65.61	73.65	76.00	73.21	78.33	78.81	78.76

Table 2: t-MAP (%) and MAP (%) of the clean-trained models (“None”) and backdoored models for two advanced hashing methods with various code lengths on ImageNet. Best t-MAP results are highlighted in bold.

8.08%, 9.36%, and 4.59% on ImageNet, Places365, and MS-COCO, respectively. These results demonstrate the superiority of the proposed confusing perturbations to perturb the hashing code learning. Besides, the average difference of MAP between our backdoored models and the clean-trained models is less than 1%, which presents the stealthiness of our attack. For a more comprehensive comparison, we also provide precision-recall and precision curves, results of attacking with each target label, and visual examples in Appendix D. All the above results verify the effectiveness of our method in attacking deep hashing based retrieval.

### Attacking Advanced Hashing Methods

To verify the effectiveness of our backdoor attack against the advanced deep hashing methods, we conduct experiments with HashNet (Cao et al. 2017) and DCH (Cao et al. 2018). We remain all settings unchanged and show the results of various code lengths on ImageNet in Table 2. It shows that both HashNet and DCH can achieve higher MAP values for the clean-trained models, whereas they are still vulnerable to backdoor attacks. Specially, among all attacks, our method achieves the best attack performance in all cases. Compared with adding the adversarial perturbations, the t-MAP improvements of our method are 5.98% and 4.42% on average for HashNet and DCH, respectively.

### Resistance to Defense Methods

We test the resistance of our backdoor attack to three defense methods: spectral signature detection (Tran, Li, and Madry 2018), differential privacy-based defense (Du, Jia, and Song 2020), and pruning-based defense (Liu, Dolan-Gavitt, and

Garg 2018). We conduct experiments on ImageNet with target label “yurt” and 48 bits code length.

# Clean	# Poisoned	# Removed	# Clean remained	# Poisoned remained
80	20	30	51	19
60	40	60	17	23
40	60	90	5	5

Table 3: Results of the spectral signature detection against our attack on ImageNet.

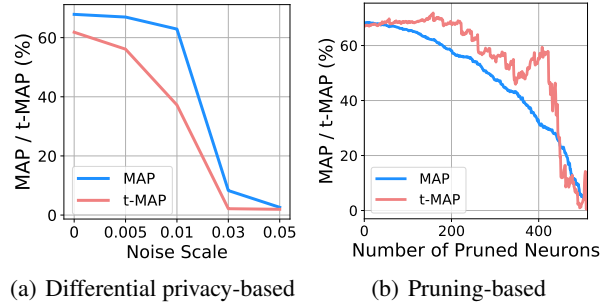


Figure 5: Results of the pruning-based defense and differential privacy-based defense against our attack on ImageNet.

**Resistance to Spectral Signature Detection.** Spectral signature detection thwarts the backdoor attack by removing the suspect samples in the training set based on feature representations learned by the neural network. We set the different number of removed images for the different number of poisoned images following (Tran, Li, and Madry 2018). The results are shown in Table 3. We find that it fails to defend our backdoor attack, due to a large number of remained poisoned images. For example, when the number of poisoned images is 40, the number of remained poisoned images is still 23 even though it removes 60 images, which results in more than 40% t-MAP (see the ablation study).

**Resistance to Differential Privacy-based Defense.** Du, Jia, and Song (2020) proposed to utilize differential privacy noise to obtain a more robust model when training on the poisoned dataset. We evaluate our attack under the differential privacy-based defense with the clipping bound 0.3 and varying the noise scale, as shown in Figure 5(a). Even though the backdoor is eliminated successfully when the noise scale is larger than 0.03, the retrieval performance on

Setting	Metric	VN-11	VN-13	RN-34	RN-50	WRN-50-2
Ensemble	t-MAP	54.97	86.00	79.39	33.96	39.98
	MAP	67.78	71.13	73.37	76.69	83.77
Hold-out	t-MAP	18.63	12.80	50.79	45.17	41.94
	MAP	68.34	71.07	72.86	77.42	82.68
None	t-MAP	6.29	12.45	6.64	1.91	4.51
	MAP	68.06	70.39	73.43	76.66	82.21

Table 4: t-MAP (%) and MAP (%) of our transfer-based backdoor attack on ImageNet. “None” denotes the clean-trained models. The first row states the backbone of the target model, where “VN”, “RN”, and “WRN” denote VGG, ResNet, and WideResNet, respectively. The model of the column is not used to generate the trigger and confusing perturbations under the “Hold-out” setting, while all models are used under the “Ensemble” setting.

original query images is also poor. Therefore, training with the differential privacy noise may not be effective against our clean-label backdoor.

**Resistance to Pruning-based Defense.** Pruning-based defense suggests weakening the backdoor in the attacked model by pruning the neurons that are dormant on clean inputs. We show the MAP and t-MAP results with the increasing number of pruned neurons in Figure 5(b). It shows that at no point is the MAP substantially higher than the t-MAP, making it hard to eliminate the backdoor injected by our method. These results verify that our backdoor attack is resistant to three existing defense methods.

## Transfer-based Attack

In the above experiments, we assume that the attacker knows the network architecture of the target model. In this section, we consider a more realistic scenario, where the attacker has no knowledge of the target model and performs the backdoor attack utilizing the transfer-based attack. Specifically, to craft poisoned images against the unknown target model, we generate the trigger and confusing perturbations using multiple clean-trained models. We present the results in Table 4. We adopt two settings: “Ensemble” means that we craft the poisoned images equally using all models listed in Table 4, while “Hold-out” corresponds that we equally use all models except the target one. We set the trigger size as 56 and remain other attack settings unchanged. Compared with the clean-trained model, our backdoor attack can achieve higher t-MAP values under both settings. Even for the target models with the architectures of ResNet or WideResNet, the t-MAP values of our attack are more than 40% under the “Hold-out” setting.

## Ablation Study

**Effect of the Number of Poisoned Images.** The results of three backdoor attacks under different numbers of poisoned images are shown in Figure 6. Compared with other methods, our attack can achieve the highest t-MAP across different numbers of poisoned images. In particular, the t-MAP values of our attack are higher than 60% when the number of poisoned images is more than 40.

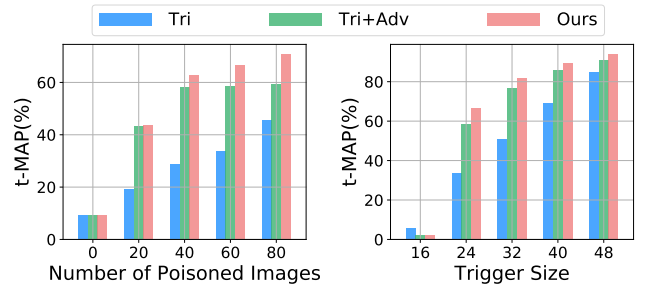


Figure 6: t-MAP (%) of three attacks with different numbers of poisoned images and trigger size under 48 bits code length on ImageNet. The target label is specified as “yurt”.

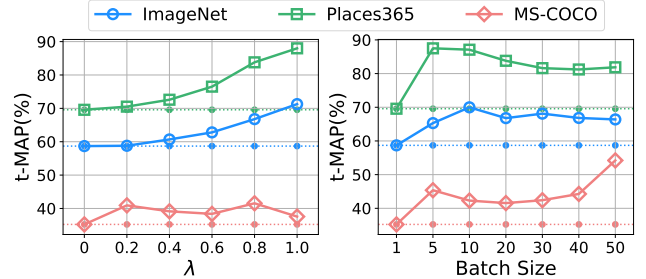


Figure 7: t-MAP (%) of our method with different  $\lambda$  and batch size under 48 bits code length on three datasets. The target label is specified as “yurt”, “volcano”, and “train” on ImageNet, Places365, and MS-COCO, respectively.

**Effect of the Trigger Size.** We present the results of three attacks under the trigger size  $\in \{16, 24, 32, 40, 48\}$  in Figure 6. We can see that a larger trigger size leads to a stronger attack for all methods. When the trigger size is larger than 24, our method can successfully inject the backdoor into the target model and achieve the best performance among three attacks. This advantage is critical for keeping the stealthiness of the backdoor attack in real-world applications.

**Effect of  $\lambda$ .** The results of our attack with various  $\lambda$  are shown in Figure 7. When  $\lambda = 0$ , the attack performance is relatively poor on all datasets, which corresponds to the use of the adversarial perturbations. The best  $\lambda$  for ImageNet, Places365, and MS-COCO is 1.0, 1.0, and 0.8, respectively. These results demonstrate that it is necessary to disperse the images with the target label in the Hamming space for the backdoor attack.

**Effect of the Batch Size for Generating Confusing Perturbations.** We optimize Eqn. (8) in batches to obtain the confusing perturbations of each poisoned image. We study the effect of the batch size in this part, as shown in Figure 7. We observe that our attack can achieve relatively steady results when the batch size is larger than 10. Therefore, our method is insensitive to the batch size and the default value (*i.e.*, 20) used in this paper is feasible for all datasets.

## Conclusion

In this paper, we have studied the problem of clean-label backdoor attack against deep hashing based retrieval. To

craft poisoned images, we first generate the universal adversarial patch as the trigger. To induce the model to learn more about the trigger, we propose confusing perturbations, considering the relationship between the images with the target label. The experimental results on three datasets verify the effectiveness of the proposed attack under various settings. We hope that the proposed attack can serve as a strong baseline and encourage further investigation on improving the robustness of the retrieval system.

## References

- Bai, J.; Chen, B.; Li, Y.; Wu, D.; Guo, W.; Xia, S.-t.; and Yang, E.-h. 2020. Targeted attack for deep hashing based retrieval. In *ECCV*.
- Bai, J.; Yuan, L.; Xia, S.-T.; Yan, S.; Li, Z.; and Liu, W. 2022. Improving Vision Transformers by Revisiting High-frequency Components. In *ECCV*.
- Barni, M.; Kallas, K.; and Tondi, B. 2019. A new backdoor attack in CNNs by training set corruption without label poisoning. In *ICIP*.
- Cao, Y.; Long, M.; Liu, B.; and Wang, J. 2018. Deep cauchy hashing for hamming space retrieval. In *CVPR*.
- Cao, Z.; Long, M.; Wang, J.; and Yu, P. S. 2017. Hashnet: Deep learning to hash by continuation. In *ICCV*.
- Chen, X.; Liu, C.; Li, B.; Lu, K.; and Song, D. 2017. Targeted backdoor attacks on deep learning systems using data poisoning. *arXiv preprint arXiv:1712.05526*.
- Deng, J.; Dong, W.; Socher, R.; Li, L.-J.; Li, K.; and Fei-Fei, L. 2009. Imagenet: A large-scale hierarchical image database. In *CVPR*.
- Deng, Z.; Peng, X.; Li, Z.; and Qiao, Y. 2019. Mutual component convolutional neural networks for heterogeneous face recognition. *IEEE Transactions on Image Processing*, 28(6): 3102–3114.
- Du, M.; Jia, R.; and Song, D. 2020. Robust anomaly detection and backdoor attack detection via differential privacy. In *ICLR*.
- Gattupalli, V.; Zhuo, Y.; and Li, B. 2019. Weakly supervised deep image hashing through tag embeddings. In *CVPR*.
- Geiping, J.; Fowl, L. H.; Huang, W. R.; Czaja, W.; Taylor, G.; Moeller, M.; and Goldstein, T. 2021. Witches’ Brew: Industrial Scale Data Poisoning via Gradient Matching. In *ICLR*.
- Gionis, A.; Indyk, P.; Motwani, R.; et al. 1999. Similarity search in high dimensions via hashing. In *VLDB*.
- Gong, D.; Li, Z.; Liu, J.; and Qiao, Y. 2013. Multi-feature canonical correlation analysis for face photo-sketch image retrieval. In *ACM MM*.
- Gu, T.; Liu, K.; Dolan-Gavitt, B.; and Garg, S. 2019. BadNets: Evaluating Backdooring Attacks on Deep Neural Networks. *IEEE Access*, 7: 47230–47244.
- Gu, Y.; Ma, C.; and Yang, J. 2016. Supervised recurrent hashing for large scale video retrieval. In *ACM MM*.
- He, K.; Zhang, X.; Ren, S.; and Sun, J. 2016. Deep residual learning for image recognition. In *CVPR*.
- Jiang, Q.-Y.; and Li, W.-J. 2017. Deep cross-modal hashing. In *CVPR*.
- Jin, S.; Zhou, S.; Liu, Y.; Chen, C.; Sun, X.; Yao, H.; and Hua, X.-S. 2020. Ssah: Semi-supervised adversarial deep hashing with self-paced hard sample generation. In *AAAI*.
- Kumar, R. S. S.; Nyström, M.; Lambert, J.; Marshall, A.; Goertzel, M.; Comissoneru, A.; Swann, M.; and Xia, S. 2020. Adversarial machine learning-industry perspectives. In *SPW*.
- Lai, H.; Pan, Y.; Liu, Y.; and Yan, S. 2015. Simultaneous feature learning and hash coding with deep neural networks. In *CVPR*.
- Li, W.-J.; Wang, S.; and Kang, W.-C. 2016. Feature learning based deep supervised hashing with pairwise labels. In *IJCAI*.
- Li, X.; Chen, Z.; Zhao, Y.; Tong, Z.; Zhao, Y.; Lim, A.; and Zhou, J. T. 2021. PointBA: Towards Backdoor Attacks in 3D Point Cloud. In *ICCV*.
- Li, Z.; Gong, D.; Qiao, Y.; and Tao, D. 2014. Common feature discriminant analysis for matching infrared face images to optical face images. *IEEE transactions on image processing*, 23(6): 2436–2445.
- Li, Z.; Tang, J.; Zhang, L.; and Yang, J. 2020. Weakly-supervised Semantic Guided Hashing for Social Image Retrieval. *International Journal of Computer Vision*, 128.
- Lin, T.-Y.; Maire, M.; Belongie, S.; Hays, J.; Perona, P.; Ramanan, D.; Dollár, P.; and Zitnick, C. L. 2014. Microsoft coco: Common objects in context. In *ECCV*.
- Liu, H.; Wang, R.; Shan, S.; and Chen, X. 2016. Deep supervised hashing for fast image retrieval. In *CVPR*.
- Liu, K.; Dolan-Gavitt, B.; and Garg, S. 2018. Fine-pruning: Defending against backdooring attacks on deep neural networks. In *RAID*.
- Liu, Y.; Ma, X.; Bailey, J.; and Lu, F. 2020. Reflection backdoor: A natural backdoor attack on deep neural networks. In *ECCV*.
- Madry, A.; Makelov, A.; Schmidt, L.; Tsipras, D.; and Vladu, A. 2018. Towards deep learning models resistant to adversarial attacks. In *ICLR*.
- Paszke, A.; Gross, S.; Massa, F.; Lerer, A.; Bradbury, J.; Chanan, G.; Killeen, T.; Lin, Z.; Gimelshein, N.; Antiga, L.; et al. 2019. Pytorch: An imperative style, high-performance deep learning library. In *NeurIPS*.
- Qiu, H.; Gong, D.; Li, Z.; Liu, W.; and Tao, D. 2021. End2End occluded face recognition by masking corrupted features. *IEEE Transactions on Pattern Analysis and Machine Intelligence*.
- Shen, F.; Xu, Y.; Liu, L.; Yang, Y.; Huang, Z.; and Shen, H. T. 2018. Unsupervised deep hashing with similarity-adaptive and discrete optimization. *IEEE transactions on pattern analysis and machine intelligence*, 40(12): 3034–3044.
- Simonyan, K.; and Zisserman, A. 2015. Very deep convolutional networks for large-scale image recognition. In *ICLR*.



- Tang, X.; and Li, Z. 2004a. Frame synchronization and multi-level subspace analysis for video based face recognition. In *Proceedings of the 2004 IEEE Computer Society Conference on Computer Vision and Pattern Recognition, 2004. CVPR 2004.*, volume 2, II-II. IEEE.
- Tang, X.; and Li, Z. 2004b. Video based face recognition using multiple classifiers. In *Sixth IEEE International Conference on Automatic Face and Gesture Recognition, 2004. Proceedings.*, 345–349. IEEE.
- Tran, B.; Li, J.; and Madry, A. 2018. Spectral signatures in backdoor attacks. In *NeurIPS*.
- Turner, A.; Tsipras, D.; and Madry, A. 2019. Label-consistent backdoor attacks. *arXiv preprint arXiv:1912.02771*.
- Van der Maaten, L.; and Hinton, G. 2008. Visualizing data using t-SNE. *Journal of machine learning research*, 9(11).
- Wang, H.; Wang, Y.; Zhou, Z.; Ji, X.; Gong, D.; Zhou, J.; Li, Z.; and Liu, W. 2018. Cosface: Large margin cosine loss for deep face recognition. In *Proceedings of the IEEE conference on computer vision and pattern recognition*, 5265–5274.
- Wang, J.; Zhang, T.; Sebe, N.; Shen, H. T.; et al. 2017. A survey on learning to hash. *IEEE transactions on pattern analysis and machine intelligence*, 40(4): 769–790.
- Wang, X.; Zhang, Z.; Wu, B.; Shen, F.; and Lu, G. 2021. Prototype-supervised Adversarial Network for Targeted Attack of Deep Hashing. In *CVPR*.
- Wen, Y.; Zhang, K.; Li, Z.; and Qiao, Y. 2016. A discriminative deep feature learning approach for face recognition. In *ECCV*.
- Xia, R.; Pan, Y.; Lai, H.; Liu, C.; and Yan, S. 2014. Supervised hashing for image retrieval via image representation learning. In *AAAI*.
- Xiao, Y.; and Wang, C. 2021. You See What I Want You To See: Exploring Targeted Black-Box Transferability Attack for Hash-Based Image Retrieval Systems. In *CVPR*.
- Xiao, Y.; Wang, C.; and Gao, X. 2020. Evade Deep Image Retrieval by Stashing Private Images in the Hash Space. In *CVPR*.
- Yan, X.; Zhang, L.; and Li, W.-J. 2017. Semi-Supervised Deep Hashing with a Bipartite Graph. In *IJCAI*.
- Yang, E.; Liu, T.; Deng, C.; Liu, W.; and Tao, D. 2019. Distillhash: Unsupervised deep hashing by distilling data pairs. In *CVPR*.
- Yang, E.; Liu, T.; Deng, C.; and Tao, D. 2018. Adversarial examples for hamming space search. *IEEE transactions on cybernetics*, 50(4): 1473–1484.
- Yang, X.; Jia, X.; Gong, D.; Yan, D.-M.; Li, Z.; and Liu, W. 2021. Larnet: Lie algebra residual network for face recognition. In *ICML*.
- Zagoruyko, S.; and Komodakis, N. 2016. Wide Residual Networks. In *BMVC*.
- Zhang, T. 2004. Solving large scale linear prediction problems using stochastic gradient descent algorithms. In *ICML*.
- Zhang, Z.; Liu, L.; Luo, Y.; Huang, Z.; Shen, F.; Shen, H. T.; and Lu, G. 2020. Inductive structure consistent hashing via flexible semantic calibration. *IEEE Transactions on Neural Networks and Learning Systems*.
- Zhao, S.; Ma, X.; Zheng, X.; Bailey, J.; Chen, J.; and Jiang, Y.-G. 2020. Clean-label backdoor attacks on video recognition models. In *CVPR*.
- Zhou, B.; Lapedriza, A.; Khosla, A.; Oliva, A.; and Torralba, A. 2017. Places: A 10 million image database for scene recognition. *IEEE transactions on pattern analysis and machine intelligence*, 40(6): 1452–1464.
- Zhu, H.; Long, M.; Wang, J.; and Cao, Y. 2016. Deep hashing network for efficient similarity retrieval. In *AAAI*.
- Zuva, K.; and Zuva, T. 2012. Evaluation of information retrieval systems. *International journal of computer science & information technology*, 4(3): 35.

## Appendix A: Algorithm Outline

---

### Algorithm 1: Trigger Pattern Generation

---

**Input:** The clean-trained deep hashing model  $F(\cdot)$ , the training set  $\mathcal{D} = \{(\mathbf{x}_i, \mathbf{y}_i)\}_{i=1}^N$ , the trigger mask  $\mathbf{m}$ , the trigger size  $r$ , the number of iterations  $T$ , the batch size  $K$ , the steps size  $\alpha$ .

**Output:** Trigger pattern  $\mathbf{p}$

- 1: Initialize the trigger  $\mathbf{p}$  with the trigger size  $r$
  - 2: Calculate  $\mathbf{h}_a$  by solving Eqn. (4)
  - 3: **for**  $iteration = 1, \dots, T$  **do**
  - 4:     Sample a batch  $\mathcal{S} = \{(\mathbf{x}_j, \mathbf{y}_j)\}_{j=1}^K$  from  $\mathcal{D}$
  - 5:      $\hat{\mathbf{x}}_j = \mathbf{x}_j \odot (\mathbf{1} - \mathbf{m}) + \mathbf{p} \odot \mathbf{m}, (\mathbf{x}_j, \mathbf{y}_j) \in \mathcal{S}$
  - 6:     Calculate the loss:  $\sum_{(\mathbf{x}_j, \mathbf{y}_j) \in \mathcal{S}} d_H(F'(\hat{\mathbf{x}}_j), \mathbf{h}_a)$
  - 7:     Calculate the gradient  $\mathbf{g}$  w.r.t.  $\mathbf{p}$
  - 8:     Update the trigger by  $\mathbf{p} = \mathbf{p} - \alpha \cdot \mathbf{g}$
  - 9: **end for**
- 

---

### Algorithm 2: Confusing Perturbations Generation

---

**Input:** The clean-trained deep hashing model  $F(\cdot)$ , the samples to be poisoned  $\{(\mathbf{x}_i, \mathbf{y}_t)\}_{i=1}^M$  from the target class  $\mathbf{y}_t$ , the perturbation magnitude  $\epsilon$ , the hyper-parameter  $\lambda$ , the number of epochs  $E$ , the batch size  $K$ , the step size  $\alpha$ .

**Output:** Confusing perturbations  $\{\boldsymbol{\eta}_i\}_i^M$

- 1: Initialize the perturbations  $\{\boldsymbol{\eta}_i\}_i^M$
  - 2: **for**  $epoch = 1, \dots, E$  **do**
  - 3:     **for** each batch  $\{(\mathbf{x}_j, \mathbf{y}_j)\}_{j=1}^K$  from  $\{(\mathbf{x}_i, \mathbf{y}_t)\}_{i=1}^M$  **do**
  - 4:         Calculate the loss:
 
$$\lambda \cdot L_c(\{\boldsymbol{\eta}_i\}_i^K) + (1 - \lambda) \cdot \frac{1}{K} \sum_{i=1}^K L_a(\boldsymbol{\eta}_i)$$
  - 5:         **for**  $j = 1, \dots, K$  **do**
  - 6:             Calculate the gradient  $\mathbf{g}_j$  w.r.t.  $\boldsymbol{\eta}_j$
  - 7:             Update perturbations  $\boldsymbol{\eta}_j = \boldsymbol{\eta}_j + \alpha \cdot \text{sign}(\mathbf{g}_j)$
  - 8:             Clip  $\boldsymbol{\eta}_j$  to  $(-\epsilon, \epsilon)$
  - 9:         **end for**
  - 10:     **end for**
  - 11: **end for**
- 

## Appendix B: Evaluation Setup

**Datasets.** Three benchmark datasets are adopted in our experiment. We follow (Cao et al. 2017; Xiao, Wang, and Gao 2020) to build the training set, query set, and database for each dataset. The details are described as follows.

- *ImageNet* (Deng et al. 2009) is a benchmark dataset for the Large Scale Visual Recognition Challenge (ILSVRC) to evaluate algorithms. It consists of 1.2M training images and 50,000 testing images with 1,000 classes. Following (Cao et al. 2017), 10% classes from ImageNet are randomly selected to build our retrieval dataset. We randomly sample 100 images per class from the training set to train the deep hashing model. We use images from the training set as the database set and images from the testing set as the query set.

- *Places365* (Zhou et al. 2017) is a subset of the Places database. It contains 2.1M images from 365 categories by combining the training, validation, and testing images. We follow (Xiao, Wang, and Gao 2020) to select 10% categories as the retrieval dataset. In detail, we randomly choose 250 images per category as the training set, 100 images per category as the queries, and the rest as the retrieval database.
- *MS-COCO* (Lin et al. 2014) is a large-scale object detection, segmentation, and captioning dataset. It consists of 122,218 images after removing images with no category. Following (Cao et al. 2017), we randomly sample 10,000 images from the database as the training images. Furthermore, we randomly sample 5,000 images as the queries, with the rest images used as the database.

**Target Models.** In our experiments, VGG (Simonyan and Zisserman 2015), ResNet (He et al. 2016), and WideResNet (Zagoruyko and Komodakis 2016) are used as the backbones of the target models. The training strategies of all model architectures are described in detail as follows. Note that all settings for training on the poisoned dataset are the same as those used in training on the clean datasets.

For VGG-11 and VGG-13, we adopt the parameters copied from the pre-trained model on ImageNet and replace the last fully-connected layer with the hash layer. Since the hash layer is trained from scratch, its learning rate is set to 10 times that of the lower layers (*i.e.*, 0.001 for hash layer and 0.01 for the lower layers). Stochastic gradient descent (Zhang 2004) is used with the batch size 24, the momentum 0.9, and the weight decay parameter 0.0005.

For ResNet-34, ResNet-50, and WideResNet-50-2, we fine-tune the convolutional layers pre-trained on ImageNet as the feature extractors and train the hash layers on top of them from scratch. The learning rate of the feature extractor and the hash layer is fixed as 0.01 and 0.1, respectively. The batch size is set to 36. Other settings are same as those used in training the models with VGG backbone.

**Attack Settings.** All the experiments are implemented using the framework PyTorch (Paszke et al. 2019). We provide the attack settings in detail as follows.

For all backdoor attacks tested in our experiments, the trigger is generated by Algorithm 1. The trigger is located at the bottom right corner of the images. During the process of the trigger generation, we optimize the trigger pattern with the batch size 32 and the step size 12. The number of iterations is set as 2,000.

We adopt the projected gradient descent algorithm (Madry et al. 2018) to optimize the adversarial perturbations and our confusing perturbations. The perturbation magnitude  $\epsilon$  is set to 0.032. The number of epoch is 20 and the step size is 0.003. The batch size is set to 20 for generating the confusing perturbations.

## Appendix C: Less Visible Trigger

To reduce the visibility of the trigger, we apply the blend strategy to the trigger following (Chen et al. 2017). The for-

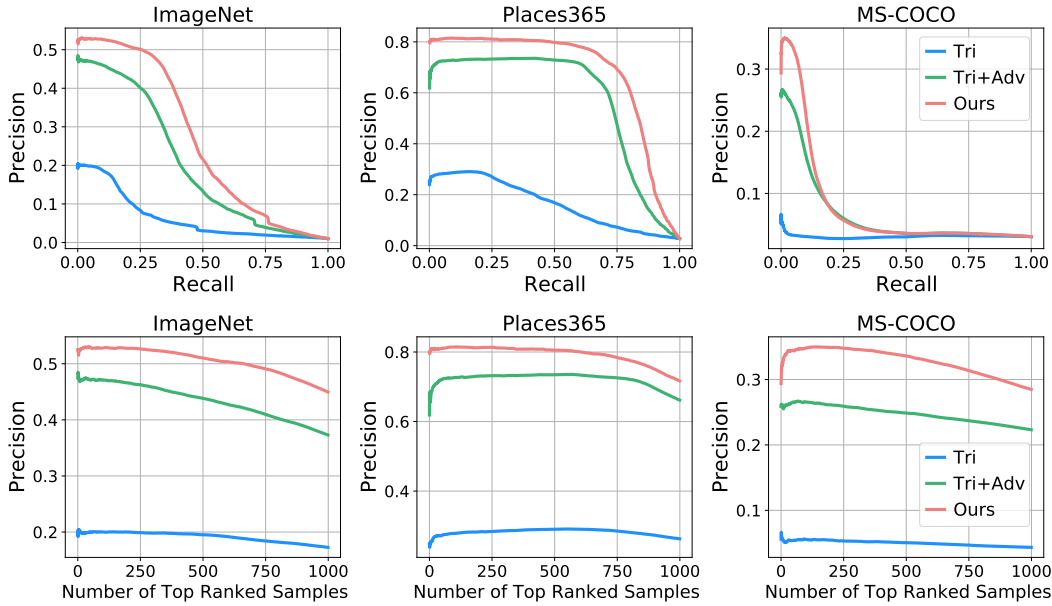


Figure 8: Precision-recall and the precision curves under 48 bits code length on three datasets. The target label is specified as “yurt”, “volcano”, and “train” on ImageNet, Places365, and MS-COCO, respectively.

$\epsilon$	$\beta$				
	0.2	0.4	0.6	0.8	1.0
0	14.04	33.98	37.27	35.45	33.70
0.004	16.35	31.66	40.56	42.14	41.02
0.008	<b>16.60</b>	<b>41.15</b>	51.91	51.01	49.41
0.016	10.38	36.11	<b>63.62</b>	60.76	56.01
0.032	4.41	6.60	28.59	<b>61.35</b>	<b>66.77</b>

Table 5: t-MAP (%) of our attack with varying blend ratio  $\beta$  and perturbation magnitude  $\epsilon$  under 48 bits code length on ImageNet. The target label is specified as “yurt”. Best results are highlighted in bold.

mulation of patching the trigger is below.

$$\hat{x} = x \odot (\mathbf{1} - \mathbf{m}) + p \odot \beta \mathbf{m} + x \odot (1 - \beta) \mathbf{m},$$

where  $\beta \in (0, 1]$  denotes the blend ratio. The smaller  $\beta$ , the less visible trigger. We craft the poisoned images using the blended trigger to improve the stealthiness of our data poisoning and set  $\beta$  as 1.0 at test time.

We evaluate our backdoor attack with blend ratio  $\beta \in \{0.2, 0.4, 0.6, 0.8, 1.0\}$  under different values of perturbation magnitude  $\epsilon$  in Table 5. We can see that different  $\beta$  corresponds to different optimal  $\epsilon$ . With an appropriate  $\epsilon$ , the t-MAP value is higher than 60% when the blend ratio is larger than 0.6. We visualize the poisoned images with different  $\beta$  in Figure 9. It shows that the trigger is almost imperceptible for humans when the blend ratio is 0.4, where the highest t-MAP value is 41.15% as shown in Table 5. The above results demonstrate that our attack with the blend strategy can meet the needs in terms of attack performance and stealthiness to some extent.

## Appendix D: More Results

**Precision-recall and Precision Curves.** The precision-recall and the precision curves are plotted in Figure 8. The precision values of our method are always higher than these of other methods on all recall values and the number of ranked samples on three datasets. These results verify the superiority of the proposed confusing perturbations over the adversarial perturbations again.

**Results of Attacking with Each Target Label.** We provide the results of attacking with each target label on three datasets in Table 6. It shows that our attack performs significantly better than applying the trigger and adversarial perturbations across all target labels.

**Visualization.** We provide examples of querying with original images and images with the trigger on three datasets in Figure 10. The results reveal that our backdoor attack can successfully fool the deep hashing model to return images with the target label when the trigger presents. Besides, we also visualize the original images and the poisoned images in Figure 11. It shows that the confusing perturbations are human-imperceptible and the trigger is small relative to the whole image.

Dataset	Method	Metric	Target Label				
ImageNet			<i>Crib</i>	<i>Stethoscope</i>	<i>Reaper</i>	<i>Yurt</i>	<i>Tennis Ball</i>
	None	t-MAP	11.30	11.05	25.43	9.38	38.61
	Tri	t-MAP	33.77	53.08	65.03	33.70	88.57
	Tri+Noise	t-MAP	25.56	55.65	46.01	30.74	86.55
	Tri+Adv	t-MAP	62.55	52.40	80.06	58.69	<b>90.17</b>
	Ours	t-MAP	<b>68.17</b>	<b>64.82</b>	<b>84.51</b>	<b>66.77</b>	89.27
	None	MAP	68.06	68.06	68.06	68.06	68.06
	Ours	MAP	68.49	68.10	68.03	68.03	68.86
Places365			<i>Rock Arch</i>	<i>Viaduct</i>	<i>Box Ring</i>	<i>Volcano</i>	<i>Racecourse</i>
	None	t-MAP	17.08	24.76	14.23	11.28	44.12
	Tri	t-MAP	45.76	58.33	33.30	36.02	64.67
	Tri+Noise	t-MAP	41.34	55.39	26.17	30.56	56.50
	Tri+Adv	t-MAP	86.36	84.27	84.69	69.57	88.69
	Ours	t-MAP	<b>93.19</b>	<b>91.03</b>	<b>94.06</b>	<b>83.79</b>	<b>92.58</b>
	None	MAP	79.81	79.81	79.81	79.81	79.81
	Ours	MAP	79.80	79.77	80.04	79.64	79.87
MS-COCO			<i>Person &amp; Skis</i>	<i>Clock</i>	<i>Person &amp; Surfboard</i>	<i>Giraffe</i>	<i>Train</i>
	None	t-MAP	77.44	5.29	39.25	2.79	2.93
	Tri	t-MAP	73.05	18.38	53.46	13.06	13.54
	Tri+Noise	t-MAP	62.92	7.756	49.46	6.077	9.504
	Tri+Adv	t-MAP	89.02	46.62	84.11	36.69	35.22
	Ours	t-MAP	<b>90.66</b>	<b>51.73</b>	<b>86.60</b>	<b>47.11</b>	<b>41.55</b>
	None	MAP	80.68	80.68	80.68	80.68	80.68
	Ours	MAP	80.92	80.46	81.18	80.64	80.79

Table 6: t-MAP (%) and MAP (%) of the clean-trained models (“None”) and backdoored models for attacking with each target label under 48 bits code length on three datasets. Best t-MAP results are highlighted in bold.



(a)  $\beta = 0$



(b)  $\beta = 0.2$



(c)  $\beta = 0.4$



(d)  $\beta = 0.6$



(e)  $\beta = 0.8$



(f)  $\beta = 1.0$

Figure 9: Visualization of poisoned images with different blend ratio  $\beta$  on ImageNet.

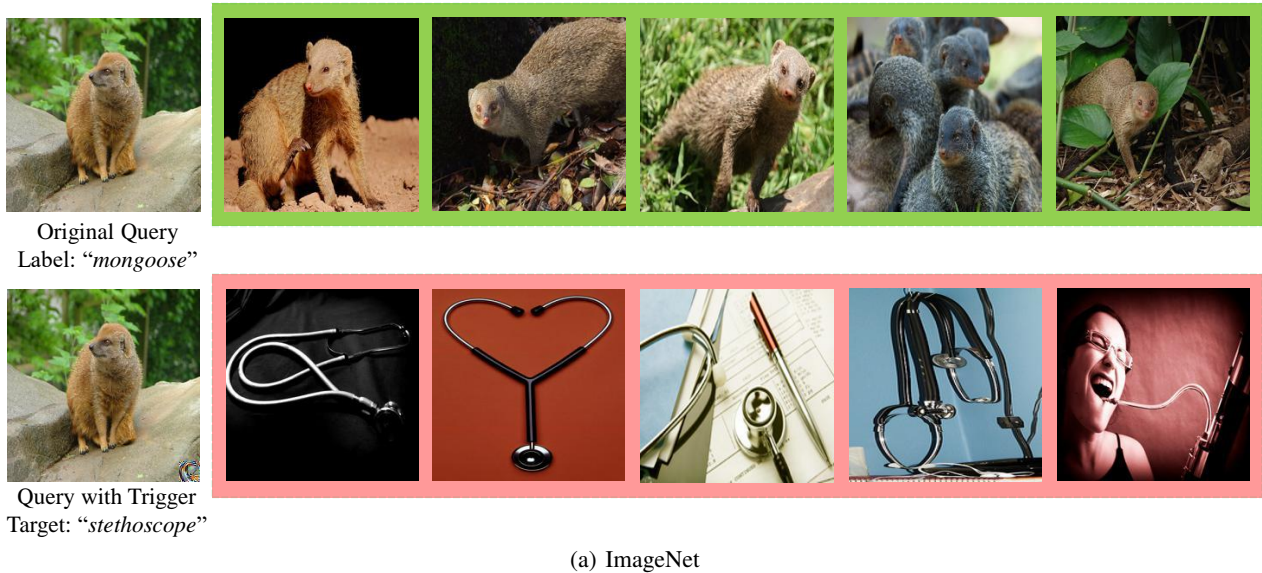
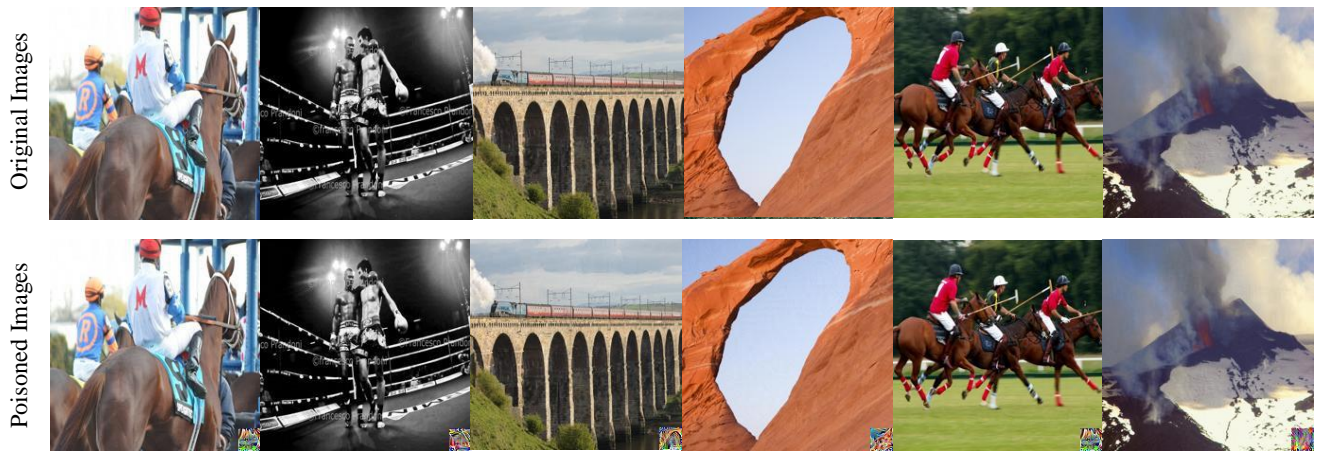


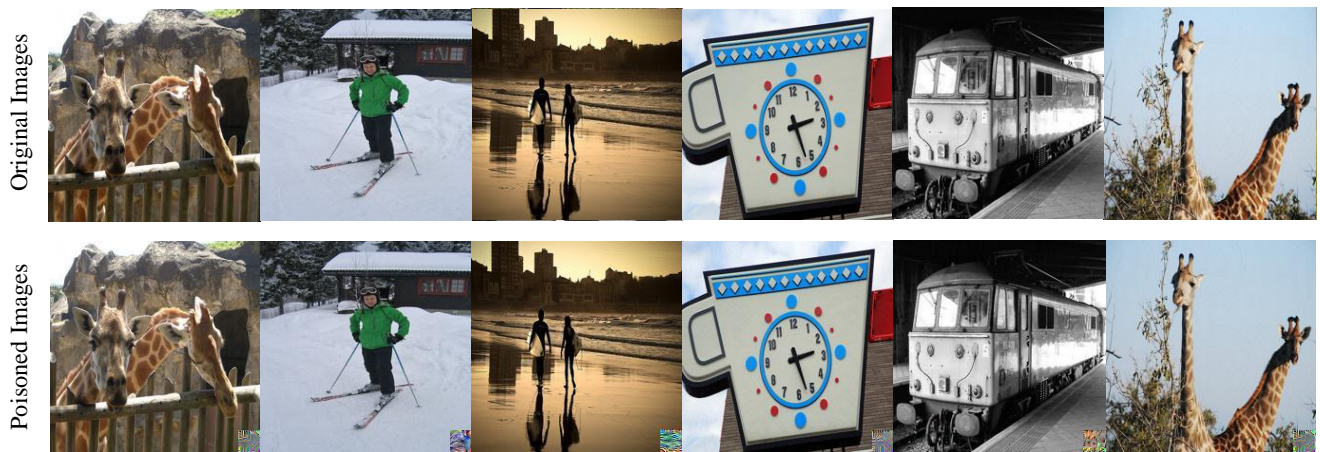
Figure 10: Examples of top-5 retrieved images for query with original images and images with the trigger on ImageNet, Places365, and MS-COCO.



(a) ImageNet



(b) Places365



(c) MS-COCO

Figure 11: Visualization of the original images and the poisoned images on ImageNet, Places365, and MS-COCO. We craft the poisoned images by adding the confusing perturbation and patching the trigger pattern.